Heat waves monitoring over West African cities: uncertainties, characterization and recent trends

Cedric G. Ngoungue Langue[1,2], Christophe Lavaysse[2,3], Mathieu Vrac[4], and Cyrille Flamant[1]

[1]Laboratoire Atmosphères, Milieux, Observations Spatiales (LATMOS) - UMR 8190 CNRS/Sorbonne Université/UVSQ, 78280 Guyancourt, France.
[2]Université Grenoble Alpes, CNRS, IRD, G-INP, IGE,38000 Grenoble, France
[3]European Commission, Joint Research Centre (JRC), 21027 Ispra, VA, Italy
[4]Laboratoire des Sciences du Climat et de l'Environnement, CEA Saclay l'Orme des Merisiers, UMR 8212 CEA-CNRS-UVSQ, Université Paris-Saclay & IPSL, 91191 Gif-sur-Yvette, France.

Correspondence: Ngoungue Langue Cedric Gacial (cedric-gacial.ngoungue-langue@latmos.ipsl.fr)

Abstract.

Heat waves can be one of the most dangerous climatic hazards affecting the planet; having dramatic impacts on the health of humans and natural ecosystems as well as on anthropogenic activities, infrastructures and economy. Based on climatic conditions in West Africa, the urban centers of the region appear to be vulnerable to heat waves. In this study, we assess the potential uncertainties encountered in the process of heat waves monitoring and analyse their recent trend in West Africa cities. This is investigated using two state-of-the-art reanalysis products namely ERA5 and MERRA for the period 1993-2020. Three types of uncertainties are discussed. The first type of uncertainty is related to the reanalyses themselves, with MERRA showing a cold bias with respect to ERA5 over the Sahel and Guinean regions except over some countries (Guinea Bissau, Sierra Leone, Liberia). Furthermore, large discrepancies are found in the representation of extreme values in the reanalyses over the southern Sahel and the Guinea coast. The second type of uncertainty is related to the sensitivity of heat waves frequency to the threshold values used to monitor them. Heat waves detected using the lowest threshold value are very persistent and last for several days; while the duration of heat waves related to high threshold values is shorter. The choice of indicators and the methodology used to define heat waves constitutes the third type of uncertainty. Three sorts of heat waves have been analysed, namely those occurring during daytime, nighttime and both daytime and nighttime concomitantly. Four indicators have been used to analyse heat waves based on 2-m temperature, humidity, 10-m wind or a combination of these. Nighttime and daytime heat waves are in the same range of occurrence while concomitant day- and nighttime events are extremely rare because they are more restrictive. The climatological state of heat wave occurrence shows large differences between the indicators. We found that humidity plays an important role in nighttime events; concomitant events associated with wet-bulb temperature are more frequent and located over the north of Sahel. Most of the events detected in the regions (75%) have a duration around 3-6 days. The most dangerous events with a duration of at least 10 days contributed up to 12% of the total number of events.For all indicators, the interannual variability of heat waves in the west Africa region evidences 4 years with a significantly higher frequency of events (1998, 2010, 2016 and 2019) possibly due to higher sea surface temperatures in the Equatorial Atlantic corresponding to El Nino events. All indicators also highlight that the cities in the Gulf of Guinea region experienced more heat waves than those lying

along the Atlantic coastline and those located in continental Sahel during the last decade. The heat wave events occurring in

25 the Guinean region show short duration and weak intensity, while in the coastal and continental regions, events are persistent with strong intensity. We find a significant increase in the frequency, duration and intensity of heat waves in cities during the last decade (2012-2020) compared to the previous two decades. This is thought to be a consequence of climate change acting on extreme events.

Keywords : heat waves, reanalysis data, climate change, climatic regions, West Africa.

30

1   Introduction

Since the industrial revolution, the Earth is experiencing a global warming around 1.5°C related to human activity ((Hartmann et al., 2013); Intergovernmental Panel on Climate Change-IPCC-report 2021). The last report of IPCC shows that this warming will exceed $1.5°C$ under different Shared Socio-economic Pathways (SSP) in 2100 if the rate of greenhouse gas emissions is

35 not reduced. This warming climate contributes to the occurrence of extreme events, but also tends to reinforce their intensity ((Fischer and Schär, 2010; Engdaw et al., 2022); IPCC report, 2021). Heat waves appear as one of the most dangerous climatic hazards affecting the planet due to their impacts on several sectors (Perkins, 2015). The health sector is the most affected; heat waves act on the thermal comfort of the body leading to an increase in morbidity, respiratory and cardiovascular diseases among the most vulnerable population (children and eldery) (e.g., Huynen et al., 2001; Braga et al., 2002; Hajat et al., 2007; Kovats and

40 Hajat, 2008; Anderson and Bell, 2009; Gasparrini and Armstrong, 2011; Rocklöv et al., 2014). Heat waves are "silent killers" because their impacts on human health are not usually instantaneous (Loughnan, 2014). In 2003, an intense heat wave occurred in France, killing more than 14000 people (Fouillet et al., 2006). During this event, temperatures sometimes reached 37°C, a record since 1950. This event was very persistent and lasted two weeks in France. In addition to this event, the Russian heat wave in 2010 caused numerous destruction (dysfunction of railway stations, interruption of energy production) and more than

45 11000 deaths (Shaposhnikov et al., 2014). Temperature sometimes reached 38°C and generated huge fires in the neighboring regions of Moscow; and a high concentration of carbon monoxide in the troposphere. In April 2010, northern Africa was affected by a severe heat wave with daily maximum temperatures frequently exceeding 40°C and daily minimum temperatures over 27°C for more than five consecutive days (Largeron et al., 2020).

Heat waves are natural disasters often associated with an increase in daytime and/or nighttime temperatures. More generally,

50 they are defined as a period of consecutive days for which the temperatures are much hotter than the normal. There is no universal formulation describing a heat wave, however a definition could be made according to the context of the study (health, environment, infrastructure, agriculture, energy supply). From a physiological point of view, the severity of a heat wave is measured through its duration and intensity.

West Africa experiences a very hot and dry climate over the Sahel region, and a hot and humid climate over the Guinea coast.
55   The climatic conditions over West Africa make the region vulnerable to heat waves when it comes to the health of humans and
natural ecosystems, but also agriculture. Many studies on heat waves have been carried out in Europe. However, heat waves in
Africa are still not well documented. Barbier et al. (2018) investigated the intraseasonal variability of large-scale heat waves
during the spring using the Berkeley Earth Surface Temperature (BEST) gridded dataset and reanalyses: the European Centre
for Medium-Range Weather Forecasts interim reanalysis (ERA-Interim), Modern-Era Retrospective analysis for Research and
60   Applications (MERRA, see section Data for more details) and the National Centers for Environmental Prediction reanalysis
(NCEP-2). They defined heat waves using anomalies of minimum/maximum values of the 2-m temperature. They found some
discrepancies in the characteristics, variability and climatic trends of heat waves in the different products. Largeron et al. (2020)
analysed the April 2010 heat wave in North Africa using both the BEST dataset and climate simulations from the atmospheric
component of the Centre National de Recherches Météorologiques (CRNM) climate model. They showed a strong link between
65   heat waves over the Sahara and the incoming heat surface fluxes. Another important result of this work, is the radiative effect
of water vapor on minimum temperatures during the heat wave period. Guigma et al. (2020) analysed the characteristics and
thermodynamics of Sahelian heat waves using different thermal indices based on temperature, wind speed, relative humidity
derived from ERA5 reanalysis (see section Data for more details). They found that most regions in the Sahel suffer on average
one or two heat waves per year with a duration of 3-5 days with severe magnitude. They have also shown that the eastern Sahel
70   experienced more frequent and longer events. They identified heat advection and greenhouse effect of moisture as the main
drivers of Sahelian heat waves. Some of the previous studies conducted over the Sahelian band, only use the daily maximum
and minimum temperatures (e.g. , Barbier et al., 2018) for the detection of heat waves, thereby ignoring the potential influence
of humidity and wind speed. Others take into account the effect of humidity in the heat wave definition (e.g. , Guigma et al.,
2020), but information about the interannual and seasonal variability of events detected are missing; even though this is very
75   important for policy makers and governments to take into account in order to develop early alert systems. Recently, Engdaw
et al. (2022) studied the trends of heat waves over Africa during the period 1980-2018 using observations from the Climate
Research Unit version 4.03 (CRU TS4.03) and BEST datasets as well as the following reanalysis datasets: ERA5, MERRA-2
and the Japanese Meteorological Agency's 55-year reanalysis (JRA-55). They highlighted large differences in both trend and
temporal evolution of heat wave indices between the different reanalyses. They found a peak of heat over northern and western
80   Africa in 2010 as well as in 2016 over eastern and southern Africa. They noticed a significant warming and an increase in
heat wave occurrence in all the regions in Africa. However, Engdaw et al. (2022) focused only on dry heat waves over a large
domain of west Africa [20°W-20°E,10°S-15°N]; the duration of heat waves were not addressed, nor the evolution of wet heat
waves.

The most lethal heat waves are not only due to high temperature, but also to the effect of humidity (Steadman, 1979a, b);
85   Hot and humid conditions (as is the case in coastal regions) can be more dangerous than equivalently hot but dry conditions
(Wehner et al., 2017). Wet heat waves, which are the most dangerous for human health, were not investigated in the previous
works. Following Steadman (1979a, b), one can legitimately wonder about the effect of humidity on the frequency of heat

waves and on the evolution of humid heat waves in west African cities. Based on previous studies, different definitions of heat wave have been proposed leading to differences in results. This is because there is no universal definition of a heat wave; based on the research objectives, some indicators and definitions can be adopted. Thereby, we can wonder about the potential sources of uncertainty found in the analysis of heat waves.

The goals of this paper are: (i) to highlight the potential uncertainties encountered in the heat wave detection process, and (ii) to analyse the recent trend and characteristics of dry and wet heat waves over a selection of West African cities grouped in climatic regions. To reach these aims, we firstly evaluate the biases in the reanalyses (ERA5 and MERRA) using ERA5 as the reference; secondly the sensitivity of heat wave occurrence respectively to the threshold values, indicators and methods applied to define heat waves are investigated. Finally, we assess the temporal variability (seasonal and interannual) of heat waves and their characteristics in different climatic regions over West Africa. The remainder of this article is organised as follows: in section 2, we present the regions of interest and the data used for this work; the description of the methodology is also provided. Section 3 contains the main results of this study following the methodology described in section 2. In section 4, the uncertainty in the reanalyses and the origin of coastal heat waves are discussed. Section 5 provides a conclusion and some perspectives for future works.

2 Region of interest, Data and Methods

2.1 Region of interest

The current study is conducted over west Africa which is located over a domain [5-20°N, 15°W-10°E], and spans from the Atlantic coast to Chad, and from the Gulf of Guinea to the southern fringes of the Sahara desert [Fig1]. The climate in west Africa is mostly influenced by the West African monsoon flux which governs the rainy season and thus the rain-fed agriculture. The West Africa region has a semi-arid and hot climate with a dry season (Koppen classification BSh or BShw). This climate corresponds to an alternation between a short wet season and a very long dry season. The West Africa region shows high climate variability at regional- and local- scale. In this study, we are interested in the coastal zone of West Africa, therefore, we identified three regions based on their location and their climate variability on which we conducted our analyses. The choice of these regions has been validated by conducting some analyses over the cities belonging to each region (not shown). The repartition of the different climatic regions is given as follows :

– Continental zone (**CONT** hereafter) including the cities of Bamako, Ouagadougou and Niamey [Fig1];

– Coastal atlantic zone (**AT** hereafter) including the cities of Dakar, Nouakchott, Monronvia and Conakry [Fig1];

– Coastal Guinean zone (**GU** hereafter) including the cities of Yamoussoukro, Abidjan, Lomé, Abuja, Lagos, Accra, Cotonou and Douala [Fig1].

2.2 Heat wave monitoring: Data and indicators

In this work, to access information with a regular spatial grid and a large horizontal coverage, we used two state-of-the-art reanalysis products: the fifth-generation European Center for Medium-Range Weather Forecasts (ECMWF) reanalysis (ERA5; (Hersbach et al., 2020)); and the Modern-Era Retrospective analysis for Research and Applications, version 2 (MERRA-2; (Gelaro et al., 2017)) from the National Oceanic Atmospheric Administration (NOAA). The spatial resolution of the products is 0.25°x0.25° and 05.°x 0.625° for ERA5 and MERRA-2, respectively. To be consistent in our analyses, we transformed the spatial resolution of MERRA-2 from 0.5°x0.625° to 0.25°x0.25° to match the one of ERA5. This is done using a first order conservative interpolation. We use hourly data covering the period going from 1 January 1993 to 31 December 2020 for all the reanalyses. We focus on atmospheric variables at the surface such as 2-meter temperature (T2m), 2-meter relative humidity (Rh), 2-meter dew-point temperature, 2-meter specific humidity, 10-meter wind components and water vapor pressure (e) from which wet bulb temperature (Tw) and Apparent Temperature (AT; (McGregor et al., 2015)) have been computed. Daily minima and maxima values were computed for T2m, Tw, AT and the Universal thermal Comfort Index (UTCI; (Di Napoli et al., 2021)). AT is similar to the heat index developed by Steadman (1984). The variables e, Tw, AT and Rh were computed using the following formulas:

$$\mathbf{e} = 6.1121 * \exp(\frac{17.502 * \mathbf{T}}{240.97 + \mathbf{T}}) \tag{1}$$

(Buck, 1981; Alduchov and Eskridge, 1996)

$$\mathbf{T_w} = \mathbf{T} * \operatorname{atan}[\mathbf{A}(\mathbf{Rh} + \mathbf{B})^{\frac{1}{2}}] + \operatorname{atan}(\mathbf{T} + \mathbf{Rh}) - \operatorname{atan}(\mathbf{Rh} - \mathbf{C}) + \mathbf{D} * (\mathbf{Rh})^{\frac{3}{2}} * (\operatorname{atan}(\mathbf{E} * \mathbf{Rh})) - \mathbf{F} \tag{2}$$

(Stull, 2011), (Rh is used in percentage, for example 32 for Rh=32

$$\mathbf{AT} = \mathbf{T_a} + 0.33 * \mathbf{e} - 0.70 * \mathbf{W_s} - 4.00 \tag{3}$$

(McGregor et al., 2015)

Rh is computed differently based on the variables available in the products. The first formula is used to compute Rh in ERA5, and the second is used for MERRA.

$$\mathbf{Rh} = 100 * \frac{\exp(\frac{\mathbf{a} * \mathbf{T_d}}{\mathbf{b} + \mathbf{T_d}})}{\exp(\frac{\mathbf{a} * \mathbf{T}}{\mathbf{b} + \mathbf{T}})} \tag{4}$$

(August, 1828; Magnus, 1844; Alduchov and Eskridge, 1996)

$$\mathbf{Rh} = \mathbf{0.263 * p * q} * [\exp(\frac{\mathbf{17.67 * (T - T_0)}}{\mathbf{T - 29.65}})]^{-1} \tag{5}$$

https://earthscience.stackexchange.com/questions/2360/how-do-i-convert-specific-humidity-to-relative-humidity

$\mathbf{a} = 17.625, \mathbf{b} = 243.04, \mathbf{A} = 0.151977, \mathbf{B} = 8.313659, \mathbf{C} = 1.676331, \mathbf{D} = 0.00391838, \mathbf{E} = 0.023101, \mathbf{F} = 4.686035, \mathbf{T_0} = 273.16 K$

Where $\mathbf{T}(°C)$, $\mathbf{T_d}(°C)$, $\mathbf{p}$(hpa) and $\mathbf{q}$ are respectively the ambient temperature, dew-point temperature, pressure and specific humidity.

2.3 Methods

2.3.1 From global to local scale : Downscaling approach

Climate models used for weather studies are generally run at global scale, therefore information at local scale is missing in many regions; this is a critical issue. To overcome this problem, downscaling methods can be used. In this work, we studied phenomena at the scale of the city while our products have much coarser spatial resolution. In this context, we need a downscaling approach to attribute variables of interest from global to local scale. Another problem we faced is that most of the cities are located along the coast and influenced by the ocean flow (see [Fig1]). The evaluation of the spatial variability of the correlation between the local scale variable (station) and reanalyses (ERA5), showed high correlation values over the continent [FigS8]. To estimate the proportion of land on a grid point, we used the land sea mask whose values range from 0 to 1. A land sea mask (lsm) of 0 means no land (a point located in the ocean), and a lsm of 1 means that the model cell is fully covered by land. Hence, to estimate the temperature over the city using reanalyses, we use the nearest grid point of reanalyses to the station which satisfies a lsm equal or greater than 0.5 (see [Table3] for lsm values of all the cities considered in this study).

2.3.2 Heat wave detection

Heat waves are usually defined as consecutive days of extremely hot temperatures above a threshold value of temperature (e.g., Tan et al., 2010; Gasparrini and Armstrong, 2011; Perkins and Alexander, 2013; Wang et al., 2019). Many factors can affect the definition of a heat wave, including the end-user sectors (human health, infrastructures, transport, agriculture) and also the climatic conditions of the regions (Perkins and Alexander, 2013). Therefore, there is no universal and standard definition of a heat wave (Perkins, 2015; Oueslati et al., 2017; Shafiei Shiva et al., 2019). Different thresholds, duration and indicators contribute to divergence in defining heat waves (Smith et al., 2013). Heat waves can be defined from daily meteorological variables such as daily raw temperature (T_{min}, T_{mean} and T_{max}) (e.g., Fontaine et al., 2013; Beniston et al., 2017; Ceccherini et al., 2017; Déqué et al., 2017; Batté et al., 2018; Barbier et al., 2018; Lavaysse et al., 2018; Engdaw et al., 2022), mean daily wet bulb temperature (Yu et al., 2021) or heat stress indices (e.g., Robinson, 2001; Fischer and Schär, 2010; Perkins et al., 2012; Guigma et al., 2020) using relative or absolute thresholds. Some other authors use the daily anomalies of temperature to define heat waves (e.g., Stefanon et al., 2012; Barbier et al., 2018). In our case, we use the daily min and max values of:

T2m ($T2m_{min}, T2m_{max}$), Tw (Tw_{min}, Tw_{max}), AT (AT_{min}, AT_{max}) and UTCI ($UTCI_{min}, UTCI_{max}$) as indicators for the detection of heat wave events. Three types of heat wave were detected (namely those occurring during daytime, nighttime and both daytime and nighttime concomitantly) using the following methods (see [Fig2]):

– **Method 1:** A heat wave is defined as a consecutive period of at least 3 days where daily max value of an indicator exceeds the calendar 90th percentile of daily max values of the indicator computed over the entire period (see HW1 in [Fig2]). This approach is useful for monitoring daytime heat wave events. Daytime events will be more associated with the incoming solar radiation;

– **Method 2:** A heat wave is defined as a consecutive period of at least 3 days where daily min value of an indicator exceeds the calendar 90th percentile of daily min values of the indicator computed over the entire period (see HW2 in [Fig2]). This approach is useful for monitoring nighttime heat wave events. Nighttime events can be related to humidity content in the region;

– **Method 3:** A heat wave is defined as a consecutive period of at least 3 days where daily min and max values of an indicator exceed the calendar 90th percentiles of daily min and max values respectively (see HW3 in [Fig2]). This method is more appropriate for extreme events that happen both during the day and the night and are very harmful for human health.

The 90th percentile is computed for each calendar day of the year using a moving window of 11 days centered on the studied day. Using a moving window, we take into account the seasonal cycle in the computation of percentiles. The use of a relative threshold is more appropriate because it can be easily reproducible in other regions. When two heat wave events are separated by one day characterized by a value of indicator below the daily 90th percentile, they are pooled together to form a single event [Fig2].

2.3.3 Heat wave characteristics

Once a heat wave is detected, some key characteristics are derived, namely duration and intensity. Some studies use the Heat Wave Magnitude Index daily (HWMId) to assess the severity of heat waves (e.g., Russo et al., 2016; Ceccherini et al., 2017). The HWMId focuses on strong heat wave events; using this metric, one cannot access the total intensity of all the events detected. In our study, the methodology applied to compute the duration and intensity of heat waves has been developed by Lavaysse et al. (2018) for the monitoring of temperature extremes over Europe. We define the heat wave mean duration as the total number of hot days in heat waves divided by the total number of heat waves over a year. Hot days are days in heat waves with daily values of the indicators above the daily thresholds. The heat wave mean duration is computed using the following expression:

$$\textbf{duration} = \frac{\textbf{1}}{\textbf{N}} \sum_{\textbf{i=1}}^{\textbf{N}} \sum_{\textbf{j}}^{\textbf{d}} \delta_{\textbf{j}} \tag{6}$$

Natural Hazards
and Earth System
Sciences
Discussions
Open Access
EGU

where $\delta_j = 1$ if $T_j >$ daily 90th percentile and $\delta_j = 0$ if $T_j <$ daily 90th percentile, N represents the total number of heatwaves per grid point and d the number of hot days.

The mean intensity of a heat wave has been defined as the sum of the daily exceedance of daily values of indicators over the daily threshold in a sequence of hot days divided by the total number of heat waves. In the scope of this study, we are interested in human impacts of heat waves, therefore we defined a constant threshold value over the whole period to compute the intensity. The expression of the intensity is given by :

$$I_1 = \frac{1}{N_{max}} * \sum_{t=1}^{T} bool_{max,t,w} * (X_{max,t,w} - min(Q_{max,w})) \tag{7}$$

$$I_2 = \frac{1}{N_{min}} * \sum_{t=1}^{T} bool_{min,t,w} * (X_{min,t,w} - min(Q_{min,w})) \tag{8}$$

$$I_3 = \frac{1}{N_{max}} * \sum_{t=1}^{T} bool_{min-max,t,w} * (X_{max,t,w} - min(Q_{max,w})) + \frac{1}{N_{min}} * \sum_{t=1}^{T} bool_{min-max,t,w} * (X_{min,t,w} - min(Q_{min,w})) \tag{9}$$

I_1, I_2, I_3 are respectively intensities associated with HW_1, HW_2, HW_3. $X_{max,t,w}, X_{min,t,w}$ are respectively daily max/min values of indicators at the grid point w $Q_{max,w}$, $Qmin, w$ represent respectively daily max/min thresholds of the indicators at the grid point w. N_{max}, N_{min} are respectively the total number of heat waves detected using max/min indicators. $bool_{max,t,w}$, $bool_{min,t,w}$ are boolean time series which contain 0 for daily values below the daily thresholds of the indicators, and 1 if daily values are above the daily thresholds respectively. $bool_{min-max,t,w}$ is a boolean time series which indicates 1 if min and max daily values of indicators are above the daily threshold, and 0 if not. T is the length in days of the study period. The mean duration and intensity are used to assess the severity of the heat wave.

2.3.4 Evaluation of the products using statistical metrics (hits, ACC, GSS)

Most regions in Africa suffer from a lack of observations due to a small number of meteorological stations available. To access information over a large domain, we use ERA5 and MERRA-2 reanalysis datasets which are very coherent in representing large-scale processes in the Saharan area (Ngoungue Langue et al., 2021). The coherence of reanalyses at regional scale has been evaluated using statistical metrics such as the probability of detection (POD), anomaly of correlation (ACC) and the Gilbert skill score (GSS).

– **POD**

The POD, also known as the "hit", is a measure of the fraction of events detected by a forecast system knowing that the events happen in the observations at the same time. It is given by the following formula :

$$\mathbf{POD} = \frac{TP}{TP + FP} \tag{10}$$

TP: True positives are events correctly detected by the two systems at the same time; FP: False positives are events not detected by the forecast system but that occured in the observations. POD values are ranging from 0 to 1; POD=1 means that all the events forecasted by the model occurred in the observations.

230 – **ACC**

The ACC is similar to a linear correlation, the only difference is that it is computed using the anomalies of variables with respect to the climatology. This metric is stricter than the simple correlation and not sensitive to the seasonal cycle which tends to increase the correlation between the products. ACC takes values between -1 and 1. ACC=1 indicates a perfect correlation between the products. For example, to compute the ACC between ERA5 and MERRA using the variable T2m in this study, we
235 firstly compute the anomalies between each reanalysis and their respective climatologies; secondly we compute the correlation between the resulting anomalies.

  – **GSS**

The GSS, known also as the equitable threat score, measures the fraction of observed events that are correctly predicted, adjusted for hits associated with random chance. The GSS does not take in account hits due to chance. It is stricter than the
240 POD; GSS takes values between $\frac{-1}{3}$ and 1. GSS=0 indicates no skill or no correlation while a GSS=1 perfect skill. Given a contingency table (see [Table2]), the computation of the GSS is done by the following formula:

$$\mathbf{GSS} = \frac{\mathbf{A} - \mathbf{CH}}{\mathbf{A} + \mathbf{B} + \mathbf{C} - \mathbf{H}} \tag{11}$$

With CH given by:

$$\mathbf{CH} = \frac{(\mathbf{A} + \mathbf{B})(\mathbf{A} + \mathbf{C})}{\mathbf{A} + \mathbf{B} + \mathbf{C} + \mathbf{D}} \tag{12}$$

245 ## 3 Results

3.1 Uncertainties in the reanalysis products

The first step of this work consists in assessing the evolution of $T2m$ in the ERA5 and MERRA reanalyses. The climatological state (annual mean) of $T2m$ in ERA5 and MERRA has been evaluated over the West Africa region from 1 January 1993 to 31 December 2020 [Fig3 a-b]. Both reanalyses show very similar climatologies of $T2m$: a north-south gradient of the
250 temperature. The Sahel region appears to be warmer than the Guinean region; this is because of the advection of cold air coming from the Atlantic ocean to the Guinea coast. This fresh air tends to cool temperatures in this region. The bias between

Natural Hazards
and Earth System
Sciences
Discussions
Open Access

EGU

ERA5 and MERRA is computed using ERA5 as reference [Fig**3** c)]. MERRA shows a cold bias with respect to ERA5 over the Sahel region and Guinean zone except in some countries (e.g., Guinea Bissau, Sierra Leone, Liberia) where we observe a hot bias. Biased values between ERA5 and MERRA are around +/-2°C. The bias highlighted between ERA5 and MERRA

255   is very significant for heat wave detection. Thereafter, we evaluate the temporal coherence between the two reanalyses by computing the ACC for T2m, AT and Tw (see [Fig**3** d-i)). We observed a weak correlation over the south of Sahel and Guinean region around 0.5 (0.7) for max (min) values of T2m and AT (see [Fig**3** d-e) and g-h)]). This could be explained by the presence of a strong diurnal cycle in the region associated with high variability during the day and less variability during the night. This will lead to a high variability in the daily max values compared to the daily min values. Tw shows a

260   uniform repartition of correlation between ERA5 and MERRA around 0.85 except in the Guinean region with max values. Good agreement between the 2 products is found with Tw. We can infer from this result that Tw has a more stable signal than T2m and AT. Knowing that heat waves are defined as extreme events, it is important to evaluate the coherence of the reanalysis products on the representation of extreme values. The hit rate and GSS have been computed using T2m, and we noticed very weak values between the two reanalysis products over the southern Sahel and Guinean region around 0.25 (see [Fig**S1**] in

265   the supplemental material). Similar results have been found with Tw (not shown). The lack of coherence between ERA5 and MERRA on the representation of extreme values would result in discrepancies on the number of heat wave events derived from the two products. The analysis of heat waves occurrence in the two products using T2m and AT shows big differences over the coastal region (see [Fig**S16**] in the supplemental material). This is very coherent with the results of the ACC correlation shown previously. These discrepancies in the reanalyses ERA5 and MERRA in West Africa have also been highlighted by

270   Engdaw et al. (2022). The potential origins of these differences are explored in the discussion section. The spatial variability of heat waves occurrence in ERA5, using T2m and AT as indicators, is very similar whatever the methods applied for heat waves detection. This strong correlation between T2m and AT is also observed when using MERRA reanalysis (see [Fig**S2**]). Even though the reanalyses present discrepancies over the south of Sahel and coastal region regarding the key variables, the correlation between the variables is preserved.

275   ## 3.2   Sensitivity of heat wave detection on the threshold values

As we have seen previously in the section "heat wave detection", the threshold value used for heat waves monitoring has a significant impact on the characteristics of the heat waves. The threshold value is related to the application we want to achieve. In this part of the work, we investigate the sensitivity of heat waves occurrence on different thresholds. To achieve this goal, we define 4 relative threshold values computed over the entire period: the $75^{th}, 80^{th}, 85^{th}$ and 90th daily percentiles. The heat

280   wave detection is processed separately for these 4 thresholds (see [Fig**S3**] Fig. S3 in the supplemental material). To quantify the changes of heat waves occurrence with respect to the threshold values, we analyse for each grid point the linear evolution of events detected and their duration. The linear evolution is computed by fitting a linear regression between the threshold values (75, 80, 85, 90) and the number of events associated to each threshold (N1, N2, N3, N4) or their corresponding duration (D1, D2, D3, D4). We are aware that this regression based on 4 points is not very robust, nevertheless it makes it possible to

285 obtain information on the evolution of the heat wave characteristics with respect to the thresholds. Therefore, we evaluated the
significance of the slope values according to the thresholds using a confidence level of 95%.

The linear evolution is given by the following equations:

$$\mathbf{N = a_w * threshold + b_w} \tag{13}$$

$$\mathbf{D = a_w^{'} * threshold + b_w^{'}} \tag{14}$$

290 where $a_w, a_w^{'}$ and $b_w, b_w^{'}$ are respectively the slopes and intercepts of the regressions for the grid point w.

This analysis is conducted with T2m and Tw extracted from MERRA and ERA5 reanalyses. We notice a high spatial
variability of the sensitivity of heat waves occurrence to the threshold values over West African regions ([Fig4] and [FigS4] in
the supplemental material). Some regions are more sensitive than the others; this can be explained by a strong seasonal cycle of
the T2m and Tw signals in those regions. We observe low changes in the heat wave occurrence and duration with respect to the

295 thresholds when using both min and max values of T2m or Tw ([Fig4 c,f)], [Fig5 c,f)] and [FigS4 c,f)] in supplement material);
this is related to the small size of the sample of events detected with method 3 (see section heat wave detection for more
details). As observed in the results, we can expect the frequency of occurrence of heat waves to increase when diminishing the
values of the threshold (see [Fig4] and [FigS3] in the supplemental material). Heat waves detected using low threshold values
are very persistent and last for several days ([Fig5] shows an illustration with T2m used as indicator). This can be explained

300 by the fact that when using a low threshold value, one may expect to have many days with temperature values above the daily
threshold. Conversely, for heat waves related to high threshold values, the duration of the events is considerably reduced. This
is statistically coherent because the number of consecutive days with temperature above the threshold will decrease as the
threshold increases. In general, we find that the duration of heat waves is more sensitive to the threshold values than their
frequency of occurrence. This is very coherent because the persistence of a heat wave will be mostly affected by the threshold

305 values used for the detection.

3.3 Sensitivity of heat wave detection to the choice of indicators and methods applied

We have shown that the heat waves detection is very sensitive to threshold values. Based on the literature review and the
application of this work, for the rest of the study, we use the 90th for heat wave analyses (e.g., Fischer and Schär, 2010;
Perkins et al., 2012; Perkins and Alexander, 2013; Fontaine et al., 2013; McGregor et al., 2015; Russo et al., 2016; Mutiibwa

310 et al., 2015; Oueslati et al., 2017; Déqué et al., 2017; Batté et al., 2018; Barbier et al., 2018; Lavaysse et al., 2018; Yu et al.,
2021; Engdaw et al., 2022) using ERA5 reanalysis as a reference. We identified four indicators: $T2m, Tw, AT$ and $UTCI$ from
which heat waves detection has been processed using three different methods (see section methods for more details) [Fig6]. We
notice that daytime and nighttime heat wave occurrences [Fig6 a-d);e-h)] are in the same range of values, while for concomitant
events [Fig6 i-l)], the occurrence of heat waves is drastically reduced by $\frac{1}{4}$. This could be explained by the fact that nighttime

315 and daytime heat waves are not necessarily occuring at the same time and their origins are totally different. Daytime heat waves will be mainly influenced by incoming solar radiation, while nighttime heat waves by the water vapor content in the air mass (Barbier et al., 2018; Largeron et al., 2020). We observe a high occurrence of nighttime heat waves over the coastal region from Guinea to Cameroon [Fig6 a-d)] linked to moist air coming from the Atlantic ocean in the region during the night; daytime heat waves are more frequent on the Sahel and north-east of Sahara [Fig6 e-h)] due to hot temperatures over the continental regions.

320 When analysing nighttime heat wave events from each indicator [Fig6 a-d)], it appears that Tw heat waves events are more frequent than $T2m/AT/UTCI$ events. Tw takes in account the effect of humidity on the temperature (see formula of Tw); it could explain the high frequency of events observed during the night in the coastal region. Regarding daytime heat waves [Fig6 e-h)], the spatial variability of events is more consistent for all the indicators in the Sahelian zone. However, some differences are observed: an increase of heat waves occurrence over the coastal region with Tw is noticed in comparison with $T2m, AT$

325 and $UTCI$. The detection of heat wave events with method 3, show that Tw events are more frequent than $T2m/AT/UTCI$ events with a maximum of occurrence located over the northern Sahel. This means that daytime and nighttime heat waves occur frequently simultaneaously in the Sahel with Tw. We can infer from this result that humidity plays a preponderant role in the occurrence of concomitant heat waves which are very dangerous for human health. In this section, we show the high sensitivity of heat waves detection on the methodology applied and the variables used as indicators. The role of humidity on

330 heat waves occurrence in the coastal region has also been highlighted.

In summary, the heat wave detection is influenced by many parameters: the dataset, threshold values, indicators and methodology used to define such an event. There is a high dependency between these parameters and the climatic region investigated. We show an illustration of the sensitivity of heat wave characteristics to the previous parameters in the CONT region [Fig12], as well as the AT and GU regions (see [FigS11] and [FigS12] in the supplemental material).

335 **3.4 Monitoring of heat waves over West Africa regions**

In this section, we analyse the spatial variability of heat wave events in three climate regions (CONT, AT and GU see section "region of interest" for more details) using $T2m$, AT and Tw as indicators and ERA5 as the reference dataset. For this purpose, we evaluate firstly the interannual variability of heat waves and their characteristics from 1993 to 2020. For each region, the characteristics of heat waves have been computed as the ratio of the sum of the characteristics of all the cities belonging

340 to a region divided by the number of cities. We identified some particular hot years with a high frequency of nighttime, daytime and concomitant heat waves: 1998, 2010, 2016 and 2019 in the 3 regions for all the indicators (see [FigS5] in the supplemental material). These years with peaks of heat waves are addressed in the discussion section. It appears that the GU region experiences more heat waves during the last decade compared to the CONT and AT regions [FigS5]; this is well marked with nighttime events (see [FigS9] in the supplemental material). The heat waves detected in the GU region have a short

345 duration and a weak intensity [Fig7]. From a statistical point of view, this is due to a high variability in the signal of indicators in the region which makes difficult the detection of consecutive days with values of indicators above the threshold. This results in many events with short duration as we observe in the GU region. Highest occurrences of heat waves in the GU region is

associated with Tw [Fig S7]. This can be explained by the fact that Tw shows a more stable signal than AT and $T2m$ in this region. Conversely, the CONT region experiences persistent and strong intensity events [Fig7 a-c) and d-f) respectively]. This
350 is explained by the fact that the CONT region presents less variability in the signal of indicators which allows detection over a long period of consecutive days with values of indicators above the threshold. The AT region has also experienced similar events as those identified in the CONT region. Strong intensity concomitant events are found in the CONT and AT regions (see [FigS6] in the supplemental material).

We also investigate the seasonal distribution of heat waves occurrence in the 3 regions. We notice an increase of the fre-
355 quency of daytime and nighttime heat waves events at the beginning of the season and during the retreat period of the West Africa monsoon (starting in September, see [FigS7] in supplement). A decrease in heat wave frequency is observed during the monsoon activity phase in the 3 regions; this is coherent because the monsoon flux brings rainfall in the region leading to a cooling effect. Concomitant heat waves show a seasonal cycle with strong fluctuations [FigS10]. This is explained by the fact that concomitant events are conditioned by daytime and nighttime heat waves which are two distinct processes. The seasonal
360 cycle of the yearly duration and intensity of heat waves follows the same distribution as the heat wave occurrence [Fig8 a,b,c)] and [Fig9 a,b,c)]. Persistent and strong intensity heat waves (nighttime, daytime) are taking place at the beginning and the end of the season, while short term and weak intensity events are occurring during the monsoon phase ([Fig8 a,b,c)], [Fig9 a,b,c)]). This is verified for all the 3 indicators in spite of some discrepancies. The period 1993-2020 is then divided into 3 three decades : [1993-2001], [2002-2011] and [2012-2020]; and we evaluate the contribution of each decade on the heat wave characteristics
365 over the whole period [Fig8 8.d,e,f) - j,k,l)] and [Fig8 9.d,e,f) - j,k,l)]. The percentiles used for the detection of heat waves in each decade are computed over the whole period 1993-2020. We notice a progressive increase in frequency (see [FigS7] in the supplemental metarial), duration and intensity of all the heat waves (daytime, nighttime and concomitant) from the first to the last decade in the 3 regions; this is true for all the indicators. The last decade [2012-2020] shows a contribution around 52% of heat wave characteristics over the period 1993-2010, while the first and second decades contribute respectively up to 21.95%
370 and 26.02%. The reinforcement of extreme events such as heat waves during the last decade is possibly being linked to global warming. This result is in agreement with other studies which show an increase of heat waves frequency and property under climate change (e.g., Dosio, 2017; Dosio et al., 2018; Murari and Ghosh, 2019; Lorenzo et al., 2021; Engdaw et al., 2022). When analysing the severity of heat waves over the previous decades using the mean duration and intensity (see [FigS14] and [FigS15]), we do not find a significant increase of heat wave characteristics over the 3 decades.

375 After assessing the temporal evolution of heat waves over the 3 regions, we analyse their persistence based on their duration. We defined 5 types of events as described in [Table2]). We observed that approximately 75% of daytime heat waves have a duration of 3-6 days with at least 40% of events belonging to C1 [Fig10]. Very persistent daytime heat waves contribute to at least 9-13% of the events registered. Severe and very severe daytime events are extremely rare in the region; and they contribute up to 12% of the total number of heat waves. The classification is not too sensitive to the indicators and the regions.
380 We obtained a similar classification with nighttime heat waves (not shown).

4 Discussion

We analyse the evolution of heat waves occurrence and characteristics over a variety of climatic regions in West Africa. The spatial variability of heat wave indicators ($T2m$ and Tw) over West Africa during the seasons (winter, spring, summer and autumn) has been investigated. This is done through the computation of the interannual daily standard deviation over the period

385   1993-2020. We find lowest values of standard deviation over the 3 regions of interest (CONT, AT and GU) during the summer and autumn when using min values of $T2m(T2m_{min})$ (see [FigS13] in the supplement material). This shows a weak variability in the signal of $T2m_{min}$ which will generate favorable conditions for the occurrence of persistent heat waves in these regions during this period. With Tw, there is a weak variability of the signal during the summer for both min and max values leading to persistent events. We find some discrepancies in the reanalysis products ERA5 and MERRA. The results show that ERA5

390   appears to be hotter than MERRA over the Sahel region. The source of these discrepancies in the reanalyses is very complex and can result from various factors such as the data assimilation techniques ($4D - Var$ (Bonavita et al., 2016) for ERA5 and $3D - Var$ (Courtier et al., 1998) for MERRA), atmospheric models, convective schemes, bias correction methods, spatial resolution and model parameterisation. Another big difference between ERA5 and MERRA is found in the vertical resolution of the profiles of the atmospheric variables between 0 and 2 km; ERA5 has more atmospheric vertical levels than MERRA

395   below 2 km which leads to more accurate representation of processes in the boundary layer (Taszarek et al., 2021). Many studies highlighted these differences in the 2 reanalysis products (e.g., Olauson, 2018; Graham et al., 2019; Taszarek et al., 2021); some authors (e.g., Gensini et al., 2014; Allen et al., 2015; Tippett et al., 2014; Taszarek et al., 2018; King and Kennedy, 2019) identified the model parameterisation and data assimilation technique as possible causes of biases in reanalyses for low level thermodynamic fields. The investigation in more details of the source of these uncertainties is out of the scope of this

400   paper.

An assessment of the origins of heat waves in the West African coastal regions is discussed. One driver of heat waves over the globe mainly in the two hemispheres, highlighted by many studies, is the "blocking high" (e.g., Charney and DeVore, 1979; Coughlan, 1983; Perkins, 2015). This situation happens when a high pressure system remains in the same region for a longer period than what is usually expected. The consequence of this phenomenon is the compression of the air mass at the surface

405   leading to an increase of temperatures in the region. Perkins (2015) also identified soil moisture-atmosphere interactions and large-scale climate dynamics as other drivers of heat waves. To address the origin of heat waves in the coastal region, we analysed the interannual variability of the sea surface temperature (sst) over the period 1993-2020. We computed the mean anomalies of sst with respect to the climatology [Fig11]. A warming over the north-eastern and south-eastern tropical Atlantic ocean is observed during specific years: 1998, 2008, 2010, 2016, 2019 and 2020. This warming over the tropical Atlantic ocean

410   is affecting all the western Africa coastal region. In comparison with the interannual variability of heat waves occurrence in the coastal region (see [FigS5] in the supplemental material), we noticed that the years of high frequency of heat waves correspond to the years during which a warming of the ocean was observed : 1998, 2010, 2016 , 2019 for instance. These years also correspond to the occurrence of El nino events. We can suggest from this result that there is a contribution of oceanic forcings

in the reinforcement of heat waves in the coastal region. This result is in agreement with Russo et al. (2016). The investigation

415   of the origins of heat waves in the coastal region required more knowledge about local- and large-scale forcings which is out of the scope of this paper.

5   Conclusions

The present work assesses the potential uncertainties associated with heat waves detection using reanalysis data sets. It also looks into the recent evolution of heat waves in different parts of the West Africa region.

420   The first uncertainty highlighted in this study is coming from the reanalyses ERA5 and MERRA. We found biases in the reanalysis products; MERRA shows a cold bias with respect to ERA5 over the Sahel region and the Guinean region except over some countries (Guinea Bissau, Sierra Leone, Liberia). Weak correlations between ERA5 and MERRA have been found over the Guinea coast using min/max values of $T2m$ and AT indicators. The representation of extreme values in the reanalyses has been analyzed, evidencing that the coherence between the 2 products is very low, around 0.25, in the southern Sahel and

425   the Guinean region. This low agreement between the 2 reanalyses results in discrepancies on the frequency of heat waves associated with each product. Even though the reanalyses present large discrepancies over the South Sahel and Guinea coast, they are able to preserve the relationship between the variables used to detect heat waves (AT, $T2m$). The second uncertainty found here, is the sensitivity of the spatial variability of heat waves to the threshold values used to process the monitoring of events. Heat waves detected using low threshold values of the indicators $T2m$ and Tw are very persistent and last for

430   several days, while the duration of heat waves related to the high threshold values is considerably reduced. We notice some discrepancies in the sensitivity to the threshold values of heat waves detected with Tw and $T2m$. Nighttime and daytime heat waves are in the same range of occurrence while concomitant events are extremely rare because they are more restrictive. This shows daytime and nighttime heat waves are distinct phenomena. The climatological state of heat wave occurrence shows large differences between the indicators. Nighttime heat waves associated to Tw are more frequent than the ones detected

435   with AT, $T2m$, $UTCI$. Humidity plays an important role in nighttime events and tends to reinforce concomitant events over the north Sahel. The spatial variability of daytime heat waves is more consistent for all the indicators over the Sahelian zone. The interannual variability of heat waves in the west Africa coastal region shows for the 3 indicators (AT, $T2m$, Tw) some particularly hotter years with high frequency of events : 1998, 2010, 2016 and 2019 linked to El Nino events. The GU region is more affected by heatwaves than the CONT and AT regions. CONT and AT regions experienced longer duration and stronger

440   intensity heat waves than the GU region. The seasonal cycle of heat waves shows an increase of the frequency of the events at the beginning of the season and during the retreat phase of the west African monsoon. Conversely, a decrease of heat waves occurrence is observed during the monsoon activity period in the 3 regions. We observed a reinforcement in the frequency, duration and intensity of heat waves during the last decade (2012-2020). This is a consequence of global warming acting on extreme events. No significant changes on the severity of heat waves have been found in the regions during the 3 decades. Most

445   of the events detected in the regions (75%) have a duration around 3-6 days. The most dangerous events with a duration of at least 10 days contributed up to 12% of the total number of events. We noticed strong links between SST and heat waves

Natural Hazards
and Earth System
Sciences
Discussions

during some specific years (1998, 2010, 2016, 2019). We can infer from this result a contribution of oceanic forcings in the reinforcement of heat waves in the coastal region. In a future work, we will investigate in more detail the influence of oceanic forcings on heat waves over this region, and the main drivers of such events. In the present study, we detected different types

450   of heat waves based on the methodology and indicator used, it will be very important to investigate their potential impacts on human health and their activities.

Natural Hazards
and Earth System
Sciences
Discussions

EGU

References

455 Alduchov, O. A. and Eskridge, R. E.: Improved Magnus form approximation of saturation vapor pressure, Journal of Applied Meteorology and Climatology, 35, 601–609, 1996.

Allen, J. T., Tippett, M. K., and Sobel, A. H.: An empirical model relating US monthly hail occurrence to large-scale meteorological environment, Journal of Advances in Modeling Earth Systems, 7, 226–243, 2015.

Anderson, B. G. and Bell, M. L.: Weather-Related Mortality, 20, 205–213, https://doi.org/10.1097/EDE.0b013e318190ee08, 2009.

460 August, E. F.: Ueber die Berechnung der Expansivkraft des Wasserdunstes, 89, 122–137, https://doi.org/10.1002/andp.18280890511, _eprint: https://onlinelibrary.wiley.com/doi/pdf/10.1002/andp.18280890511, 1828.

Barbier, J., Guichard, F., Bouniol, D., Couvreux, F., and Roehrig, R.: Detection of Intraseasonal Large-Scale Heat Waves: Characteristics and Historical Trends during the Sahelian Spring, 31, 61–80, https://doi.org/10.1175/JCLI-D-17-0244.1, publisher: American Meteorological Society Section: Journal of Climate, 2018.

465 Batté, L., Ardilouze, C., and Déqué, M.: Forecasting West African Heat Waves at Subseasonal and Seasonal Time Scales, 146, 889–907, https://doi.org/10.1175/MWR-D-17-0211.1, publisher: American Meteorological Society Section: Monthly Weather Review, 2018.

Beniston, M., Stoffel, M., and Guillet, S.: Comparing observed and hypothetical climates as a means of communicating to the public and policymakers: The case of European heatwaves, 67, 27–34, https://doi.org/10.1016/j.envsci.2016.11.008, 2017.

Bonavita, M., Hólm, E., Isaksen, L., and Fisher, M.: The evolution of the ECMWF hybrid data assimilation system, 142, 287–303, 470 https://doi.org/10.1002/qj.2652, _eprint: https://onlinelibrary.wiley.com/doi/pdf/10.1002/qj.2652, 2016.

Braga, A. L. F., Zanobetti, A., and Schwartz, J.: The effect of weather on respiratory and cardiovascular deaths in 12 U.S. cities., 110, 859–863, https://doi.org/10.1289/ehp.02110859, publisher: Environmental Health Perspectives, 2002.

Buck, A. L.: New equations for computing vapor pressure and enhancement factor, Journal of Applied Meteorology and Climatology, 20, 1527–1532, 1981.

475 Ceccherini, G., Russo, S., Ameztoy, I., Marchese, A. F., and Carmona-Moreno, C.: Heat waves in Africa 1981–2015, observations and reanalysis, 17, 115–125, https://doi.org/10.5194/nhess-17-115-2017, 2017.

Charney, J. G. and DeVore, J. G.: Multiple flow equilibria in the atmosphere and blocking, Journal of Atmospheric Sciences, 36, 1205–1216, 1979.

Coughlan, M.: A comparative climatology of blocking action in the two hemispheres, Australian meteorological magazine Melbourne, 31, 480 3–13, 1983.

Courtier, P., Andersson, E., Heckley, W., Vasiljevic, D., Hamrud, M., Hollingsworth, A., Rabier, F., Fisher, M., and Pailleux, J.: The ECMWF implementation of three-dimensional variational assimilation (3D-Var). I: Formulation, 124, 1783–1807, https://doi.org/10.1002/qj.49712455002, _eprint: https://onlinelibrary.wiley.com/doi/pdf/10.1002/qj.49712455002, 1998.

Déqué, M., Calmanti, S., Christensen, O. B., Aquila, A. D., Maule, C. F., Haensler, A., Nikulin, G., and Teichmann, C.: A multi-model 485 climate response over tropical Africa at+ 2° C, Climate Services, 7, 87–95, 2017.

Di Napoli, C., Barnard, C., Prudhomme, C., Cloke, H. L., and Pappenberger, F.: ERA5-HEAT: A global gridded historical dataset of human thermal comfort indices from climate reanalysis, 8, 2–10, https://doi.org/10.1002/gdj3.102, _eprint: https://onlinelibrary.wiley.com/doi/pdf/10.1002/gdj3.102, 2021.

Dosio, A.: Projection of temperature and heat waves for Africa with an ensemble of CORDEX Regional Climate Models, 49, 493–519, 490 https://doi.org/10.1007/s00382-016-3355-5, 2017.

Dosio, A., Mentaschi, L., Fischer, E. M., and Wyser, K.: Extreme heat waves under 1.5\hspace0.167em°C and 2\hspace0.167em°C global warming, 13, 054 006, https://doi.org/10.1088/1748-9326/aab827, publisher: IOP Publishing, 2018.

Engdaw, M. M., Ballinger, A. P., Hegerl, G. C., and Steiner, A. K.: Changes in temperature and heat waves over Africa using observational and reanalysis data sets, International Journal of Climatology, 42, 1165–1180, 2022.

495 Fischer, E. M. and Schär, C.: Consistent geographical patterns of changes in high-impact European heatwaves, Nature geoscience, 3, 398–403, 2010.

Fontaine, B., Janicot, S., and Monerie, P.-A.: Recent changes in air temperature, heat waves occurrences, and atmospheric circulation in Northern Africa, 118, 8536–8552, https://doi.org/10.1002/jgrd.50667, _eprint: https://onlinelibrary.wiley.com/doi/pdf/10.1002/jgrd.50667, 2013.

500 Fouillet, A., Rey, G., Laurent, F., Pavillon, G., Bellec, S., Guihenneuc-Jouyaux, C., Clavel, J., Jougla, E., and Hémon, D.: Excess mortality related to the August 2003 heat wave in France, 80, 16–24, https://doi.org/10.1007/s00420-006-0089-4, 2006.

Gasparrini, A. and Armstrong, B.: The impact of heat waves on mortality, 22, 68–73, https://doi.org/10.1097/EDE.0b013e3181fdcd99, 2011.

Gelaro, R., McCarty, W., Suárez, M. J., Todling, R., Molod, A., Takacs, L., Randles, C. A., Darmenov, A., Bosilovich, M. G., Reichle, R., Wargan, K., Coy, L., Cullather, R., Draper, C., Akella, S., Buchard, V., Conaty, A., Silva, A. M. d., Gu, W., Kim, G.-K., Koster, R., Lucchesi,
505 R., Merkova, D., Nielsen, J. E., Partyka, G., Pawson, S., Putman, W., Rienecker, M., Schubert, S. D., Sienkiewicz, M., and Zhao, B.: The Modern-Era Retrospective Analysis for Research and Applications, Version 2 (MERRA-2), 30, 5419–5454, https://doi.org/10.1175/JCLI-D-16-0758.1, publisher: American Meteorological Society Section: Journal of Climate, 2017.

Gensini, V. A., Mote, T. L., and Brooks, H. E.: Severe-thunderstorm reanalysis environments and collocated radiosonde observations, Journal of Applied Meteorology and Climatology, 53, 742–751, 2014.

510 Graham, R. M., Hudson, S. R., and Maturilli, M.: Improved performance of ERA5 in Arctic gateway relative to four global atmospheric reanalyses, Geophysical Research Letters, 46, 6138–6147, 2019.

Guigma, K. H., Todd, M., and Wang, Y.: Characteristics and thermodynamics of Sahelian heatwaves analysed using various thermal indices, 55, 3151–3175, https://doi.org/10.1007/s00382-020-05438-5, 2020.

Hajat, S., Kovats, R. S., and Lachowycz, K.: Heat-related and cold-related deaths in England and Wales: who is at risk?, 64, 93–100,
515 https://doi.org/10.1136/oem.2006.029017, publisher: BMJ Publishing Group Ltd Section: Original article, 2007.

Hartmann, D. L., Tank, A. M. K., Rusticucci, M., Alexander, L. V., Brönnimann, S., Charabi, Y. A. R., Dentener, F. J., Dlugokencky, E. J., Easterling, D. R., Kaplan, A., et al.: Observations: atmosphere and surface, in: Climate change 2013 the physical science basis: Working group I contribution to the fifth assessment report of the intergovernmental panel on climate change, pp. 159–254, Cambridge University Press, 2013.

520 Hersbach, H., Bell, B., Berrisford, P., Hirahara, S., Horányi, A., Muñoz-Sabater, J., Nicolas, J., Peubey, C., Radu, R., Schepers, D., Simmons, A., Soci, C., Abdalla, S., Abellan, X., Balsamo, G., Bechtold, P., Biavati, G., Bidlot, J., Bonavita, M., De Chiara, G., Dahlgren, P., Dee, D., Diamantakis, M., Dragani, R., Flemming, J., Forbes, R., Fuentes, M., Geer, A., Haimberger, L., Healy, S., Hogan, R. J., Hólm, E., Janisková, M., Keeley, S., Laloyaux, P., Lopez, P., Lupu, C., Radnoti, G., de Rosnay, P., Rozum, I., Vamborg, F., Villaume, S., and Thépaut, J.-N.: The ERA5 global reanalysis, 146, 1999–2049, https://doi.org/10.1002/qj.3803, _eprint:
525 https://onlinelibrary.wiley.com/doi/pdf/10.1002/qj.3803, 2020.

Huynen, M. M., Martens, P., Schram, D., Weijenberg, M. P., and Kunst, A. E.: The impact of heat waves and cold spells on mortality rates in the Dutch population., 109, 463–470, https://doi.org/10.1289/ehp.01109463, publisher: Environmental Health Perspectives, 2001.

Natural Hazards
and Earth System
Sciences
Discussions

King, A. T. and Kennedy, A. D.: North American supercell environments in atmospheric reanalyses and RUC-2, Journal of Applied Meteorology and Climatology, 58, 71–92, 2019.

530   Kovats, R. S. and Hajat, S.: Heat Stress and Public Health: A Critical Review, 29, 41–55, https://doi.org/10.1146/annurev.publhealth.29.020907.090843, 2008.

Largeron, Y., Guichard, F., Roehrig, R., Couvreux, F., and Barbier, J.: The April 2010 North African heatwave: when the water vapor greenhouse effect drives nighttime temperatures, 54, 3879–3905, https://doi.org/10.1007/s00382-020-05204-7, 2020.

Lavaysse, C., Cammalleri, C., Dosio, A., van der Schrier, G., Toreti, A., and Vogt, J.: Towards a monitoring system of temperature extremes
535   in Europe, 18, 91–104, https://doi.org/10.5194/nhess-18-91-2018, publisher: Copernicus GmbH, 2018.

Lorenzo, N., Díaz-Poso, A., and Royé, D.: Heatwave intensity on the Iberian Peninsula: Future climate projections, 258, 105 655, https://doi.org/10.1016/j.atmosres.2021.105655, 2021.

Loughnan, M.: Heatwaves are silent killers, Geodate, 27, 7–10, 2014.

Magnus, G.: Versuche über die Spannkräfte des Wasserdampfs, 137, 225–247, https://doi.org/10.1002/andp.18441370202, _eprint:
540   https://onlinelibrary.wiley.com/doi/pdf/10.1002/andp.18441370202, 1844.

McGregor, G. R., Bessmoulin, P., Ebi, K., and Menne, B.: Heatwaves and health: guidance on warning-system development., WMOP, 2015.

Murari, K. K. and Ghosh, S.: Future Heat Wave Projections and Impacts, in: Climate Change Signals and Response: A Strategic Knowledge Compendium for India, edited by Venkataraman, C., Mishra, T., Ghosh, S., and Karmakar, S., pp. 91–107, Springer, https://doi.org/10.1007/978-981-13-0280-0_6, 2019.

545   Mutiibwa, D., Vavrus, S. J., McAfee, S. A., and Albright, T. P.: Recent spatiotemporal patterns in temperature extremes across conterminous United States, Journal of Geophysical Research: Atmospheres, 120, 7378–7392, 2015.

Ngoungue Langue, C. G., Lavaysse, C., Vrac, M., Peyrille, P., and Flamant, C.: Seasonal forecasts of the Saharan Heat Low characteristics: A multi-model assessment, Weather and Climate Dynamics, 2, 893–912, 2021.

Olauson, J.: ERA5: The new champion of wind power modelling?, Renewable energy, 126, 322–331, 2018.

550   Oueslati, B., Pohl, B., Moron, V., Rome, S., and Janicot, S.: Characterization of Heat Waves in the Sahel and Associated Physical Mechanisms, 30, 3095–3115, https://doi.org/10.1175/JCLI-D-16-0432.1, publisher: American Meteorological Society Section: Journal of Climate, 2017.

Perkins, S. E.: A review on the scientific understanding of heatwaves—Their measurement, driving mechanisms, and changes at the global scale, 164-165, 242–267, https://doi.org/10.1016/j.atmosres.2015.05.014, 2015.

555   Perkins, S. E. and Alexander, L. V.: On the Measurement of Heat Waves, 26, 4500–4517, https://doi.org/10.1175/JCLI-D-12-00383.1, publisher: American Meteorological Society Section: Journal of Climate, 2013.

Perkins, S. E., Alexander, L. V., and Nairn, J. R.: Increasing frequency, intensity and duration of observed global heatwaves and warm spells, 39, https://doi.org/10.1029/2012GL053361, _eprint: https://onlinelibrary.wiley.com/doi/pdf/10.1029/2012GL053361, 2012.

Robinson, P. J.: On the Definition of a Heat Wave, 40, 762–775, https://doi.org/10.1175/1520-0450(2001)040<0762:OTDOAH>2.0.CO;2,
560   publisher: American Meteorological Society Section: Journal of Applied Meteorology and Climatology, 2001.

Rocklöv, J., Forsberg, B., Ebi, K., and Bellander, T.: Susceptibility to mortality related to temperature and heat and cold wave duration in the population of Stockholm County, Sweden, 7, 22 737, https://doi.org/10.3402/gha.v7.22737, publisher: Taylor & Francis _eprint: https://doi.org/10.3402/gha.v7.22737, 2014.

Russo, S., Marchese, A. F., Sillmann, J., and Immé, G.: When will unusual heat waves become normal in a warming Africa?, 11, 054 016,
565   https://doi.org/10.1088/1748-9326/11/5/054016, publisher: IOP Publishing, 2016.

Shafiei Shiva, J., Chandler, D. G., and Kunkel, K. E.: Localized Changes in Heat Wave Properties Across the United States, 7, 300–319, https://doi.org/10.1029/2018EF001085, _eprint: https://onlinelibrary.wiley.com/doi/pdf/10.1029/2018EF001085, 2019.

Shaposhnikov, D., Revich, B., Bellander, T., Bedada, G. B., Bottai, M., Kharkova, T., Kvasha, E., Lezina, E., Lind, T., Semutnikova, E., and Pershagen, G.: Mortality Related to Air Pollution with the Moscow Heat Wave and Wildfire of 2010, 25, 359–364, https://doi.org/10.1097/EDE.0000000000000090, 2014.

Smith, T. T., Zaitchik, B. F., and Gohlke, J. M.: Heat waves in the United States: definitions, patterns and trends, 118, 811–825, https://doi.org/10.1007/s10584-012-0659-2, 2013.

Steadman, R. G.: The Assessment of Sultriness. Part I: A Temperature-Humidity Index Based on Human Physiology and Clothing Science, 18, 861–873, https://doi.org/10.1175/1520-0450(1979)018<0861:TAOSPI>2.0.CO;2, publisher: American Meteorological Society Section: Journal of Applied Meteorology and Climatology, 1979a.

Steadman, R. G.: The Assessment of Sultriness. Part II: Effects of Wind, Extra Radiation and Barometric Pressure on Apparent Temperature, 18, 874–885, https://www.jstor.org/stable/26179217, publisher: American Meteorological Society, 1979b.

Steadman, R. G.: A universal scale of apparent temperature, Journal of Applied Meteorology and Climatology, 23, 1674–1687, 1984.

Stefanon, M., D'Andrea, F., and Drobinski, P.: Heatwave classification over Europe and the Mediterranean region, 7, 014 023, https://doi.org/10.1088/1748-9326/7/1/014023, publisher: IOP Publishing, 2012.

Stull, R.: Wet-Bulb Temperature from Relative Humidity and Air Temperature, 50, 2267–2269, https://doi.org/10.1175/JAMC-D-11-0143.1, publisher: American Meteorological Society Section: Journal of Applied Meteorology and Climatology, 2011.

Tan, J., Zheng, Y., Tang, X., Guo, C., Li, L., Song, G., Zhen, X., Yuan, D., Kalkstein, A. J., Li, F., and Chen, H.: The urban heat island and its impact on heat waves and human health in Shanghai, 54, 75–84, https://doi.org/10.1007/s00484-009-0256-x, 2010.

Taszarek, M., Brooks, H. E., Czernecki, B., Szuster, P., and Fortuniak, K.: Climatological aspects of convective parameters over Europe: A comparison of ERA-Interim and sounding data, Journal of Climate, 31, 4281–4308, 2018.

Taszarek, M., Pilguj, N., Allen, J. T., Gensini, V., Brooks, H. E., and Szuster, P.: Comparison of convective parameters derived from ERA5 and MERRA-2 with rawinsonde data over Europe and North America, Journal of Climate, 34, 3211–3237, 2021.

Tippett, M. K., Sobel, A. H., Camargo, S. J., and Allen, J. T.: An empirical relation between US tornado activity and monthly environmental parameters, Journal of Climate, 27, 2983–2999, 2014.

Wang, P., Tang, J., Sun, X., Liu, J., and Juan, F.: Spatiotemporal characteristics of heat waves over China in regional climate simulations within the CORDEX-EA project, 52, 799–818, https://doi.org/10.1007/s00382-018-4167-6, 2019.

Wehner, M., Castillo, F., and Stone, D.: The impact of moisture and temperature on human health in heat waves, in: Oxford Research Encyclopedia of Natural Hazard Science, 2017.

Yu, S., Tett, S. F. B., Freychet, N., and Yan, Z.: Changes in regional wet heatwave in Eurasia during summer (1979–2017), 16, 064 094, https://doi.org/10.1088/1748-9326/ac0745, publisher: IOP Publishing, 2021.

Natural Hazards
and Earth System
Sciences
Discussions

Tables

Table 1. Contingency table.

2X2 Contingency table		Event Observed	
		YES	N0
Event forecast	YES	A	B
	NO	C	D

Table 2. Classification of heat waves based on the duration.

Classes	Duration (days)	Degree of persistence
C1	3	normal
C2	4-6	peristent
C3	7-9	very persistent
C4	10-12	severe
C5	+13	very severe

Table 3. Land sea mask (lsm) of west African towns used in this study

Towns	latitude	longitude	lsm
DAKAR	14.75	-17.25	0.6
ABIDJAN	5.25	-3.75	0.5
NOUAKCHOTT	18	-16	continent
CONAKRY	9.5	-13.5	0.5
MONROVIA	6.25	-10.75	0.6
BAMAKO	12.5	-8	continent
YAMOUSSOUKRO	6.75	-5.25	continent
OUAGADOUGOU	12.25	-1.5	continent
ACCRA	5.5	-0.5	0.8
LOMÉ	6	1	0.5
NIAMEY	13.5	2	continent
COTONOU	6.5	2.5	0.7
LAGOS	6.5	3.5	0.5
ABUJA	9	7.5	continent
DOUALA	4	9.75	0.9

Natural Hazards
and Earth System
Sciences

Discussions

Open Access

EGU
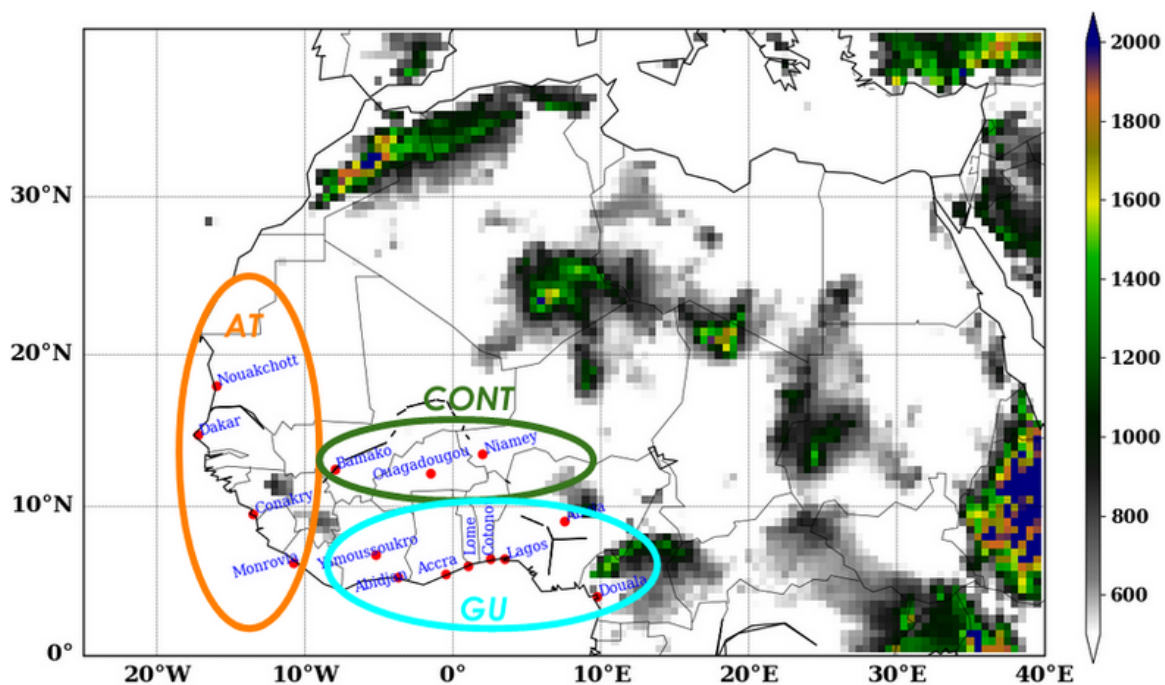
Figure 1. *Topographic map of West Africa using ERA5 elevation data. The circles on the map represent the different climatic zones: AT (Coastal atlantic zone), CONT (Continental zone) and GU (Coastal Guinean zone). The y- and x- axis represent the latitude and longitude respectively. The color bar shows the elevation in meters over the region.*
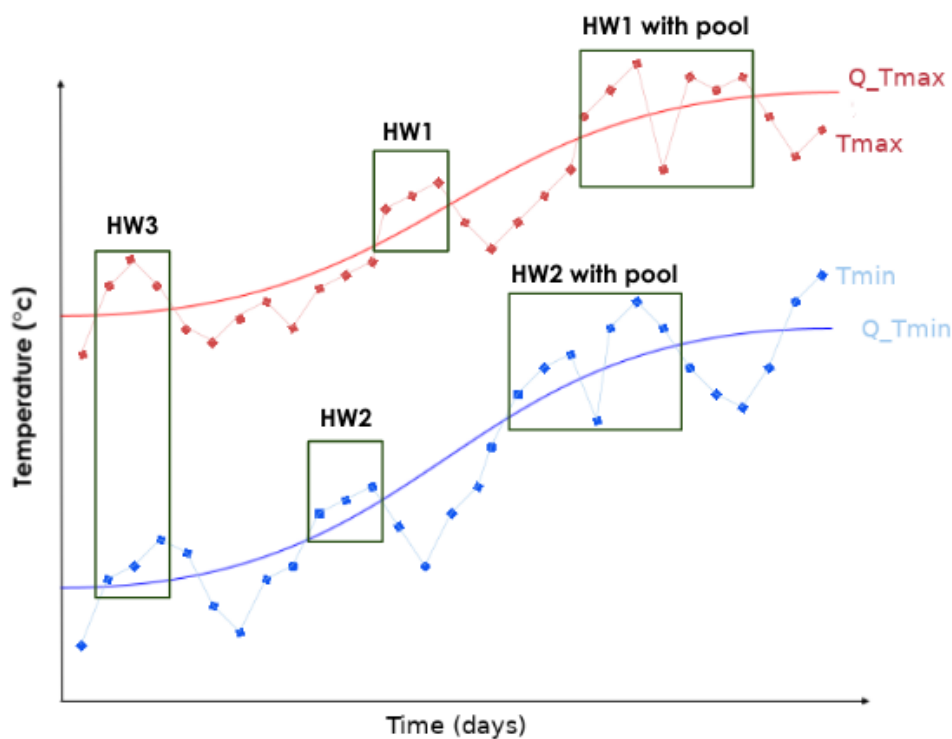
Figure 2. *Detection process of heat wave: HW1/HW2 represent events associated respectively to maxima/minima temperature, HW3 are events detected at same time in maxima and minima temperatures. The red/blue lines with circles are max/min daily temperatures. Red/blue solid lines are respectively max/min thresholds. X- and Y- axis represent the time in days and the temperature in degrees celsius. 'With pool' refers to the pooling of two (or more) events separated by a day characterized by the value of a given indicator below the daily XXth percentile.*
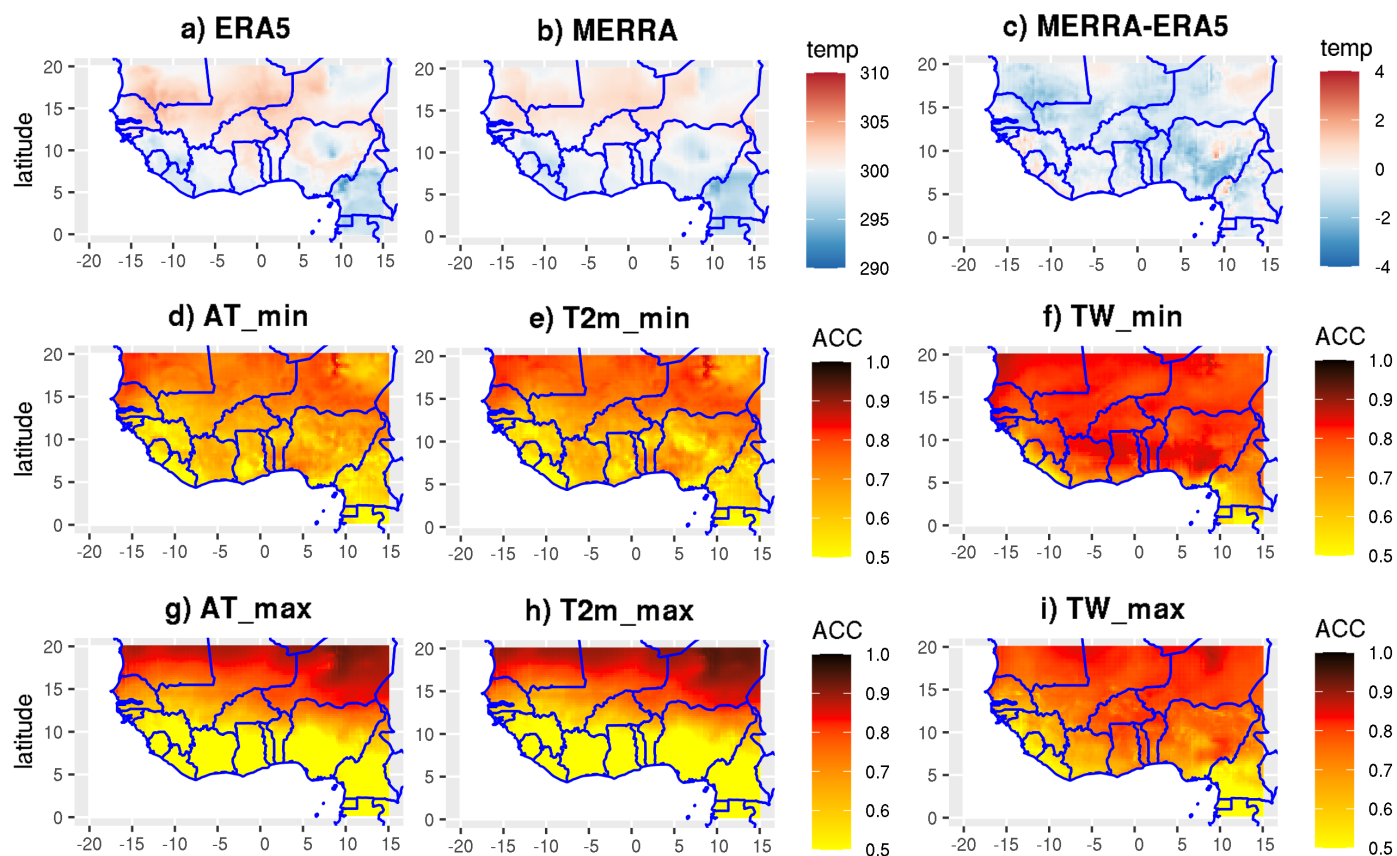
Figure 3. *Evaluation of products: a-b) Climatology state of T2m over 1993-2020 respectively for ERA5 and MERRA; c) Climatological bias between MERRA and ERA5 using ERA5 as reference. d-f) / g-i) Anomaly of correlation between MERRA and ERA5 respectively for min / max values using AT, T2m and TW variables. X and Y -axis represent respectively the longitude and latitude in degrees. The color bars show respectively the temperature (temp) in degree Kelvin and the values of anomaly of temperature (ACC).*
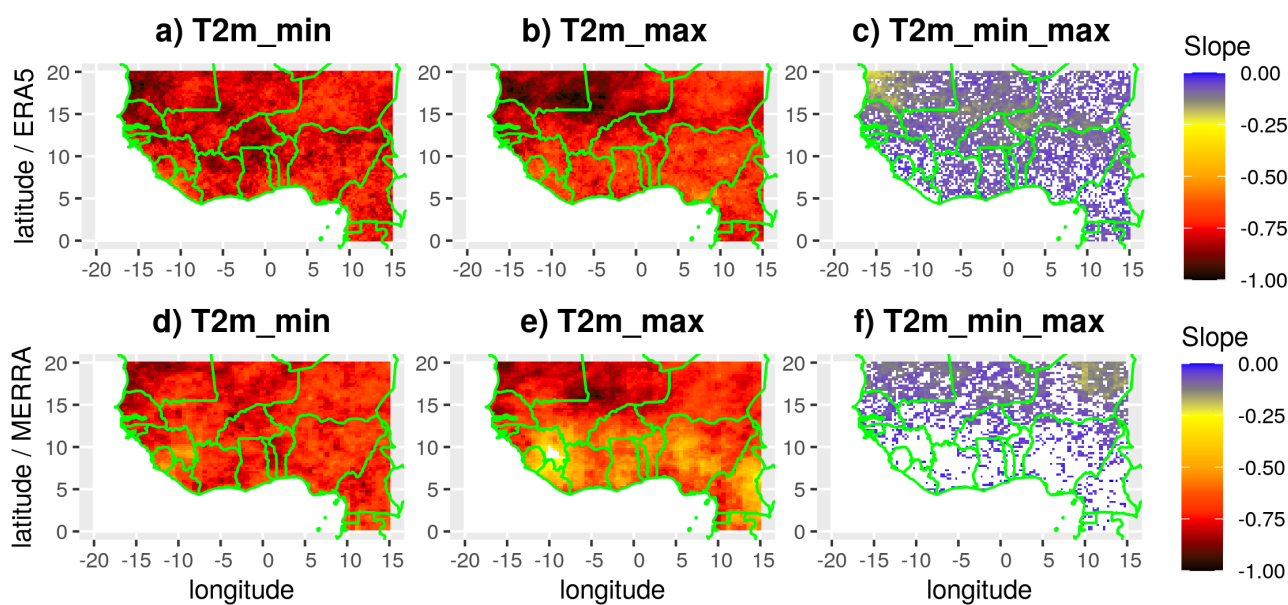
Figure 4. *Evolution of the heat wave occurrence with respect to the threshold values using T2m as indicator respectively for : a-c) ERA5 and d-f) MERRA. The slope is computed using the $75^{th}, 80^{th}, 85^{th}$ and 90th percentiles. X- and Y- axis respectively represent the longitude and latitude in degrees. The color bar shows the values of the linear evolution of the duration of heat wave per percentile. The white blanks indicate non significant changes in the occurrence of heat waves per percentile.*
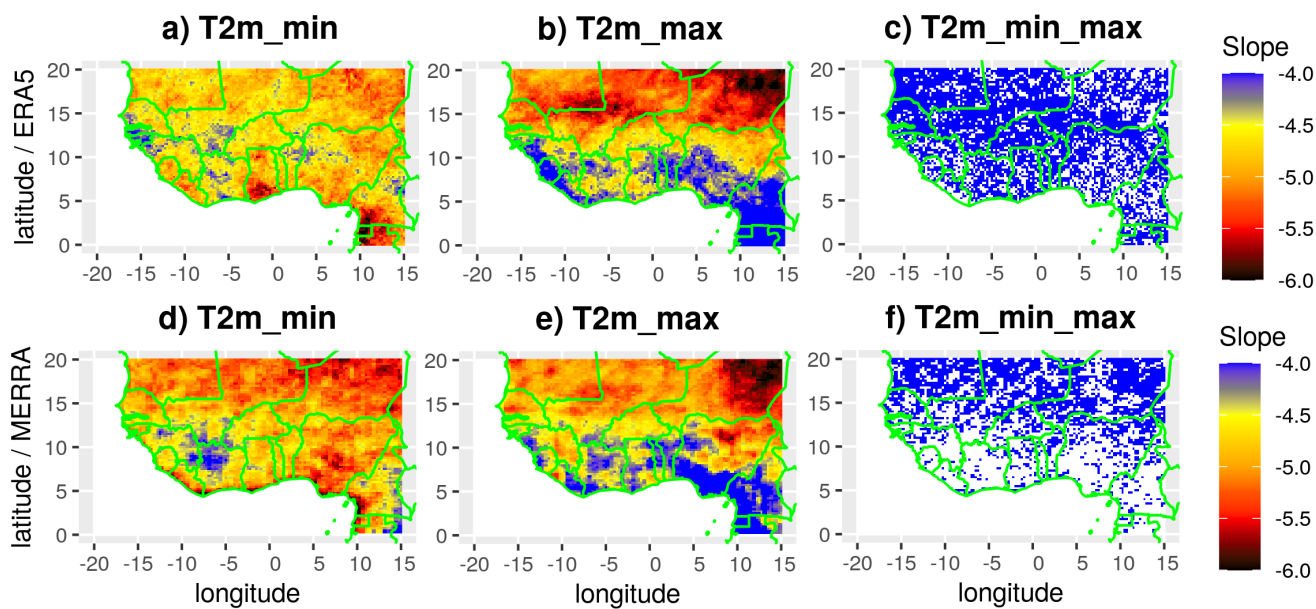
Figure 5. *Evolution of the heat wave duration with respect to the threshold values using T2m as indicator respectively for : a-c) ERA5 and d-f) MERRA. The slope is computed using the $75^{th}, 80^{th}, 85^{th}$ and 90th percentiles. X and Y-axis respectively represent the longitude and latitude in degrees. The color bar shows the values of the linear evolution of the duration of heat wave per percentile. The white blanks indicate non significant changes in the duration of heat waves per percentile.*

Natural Hazards
and Earth System
Sciences
Discussions

Open Access

EGU
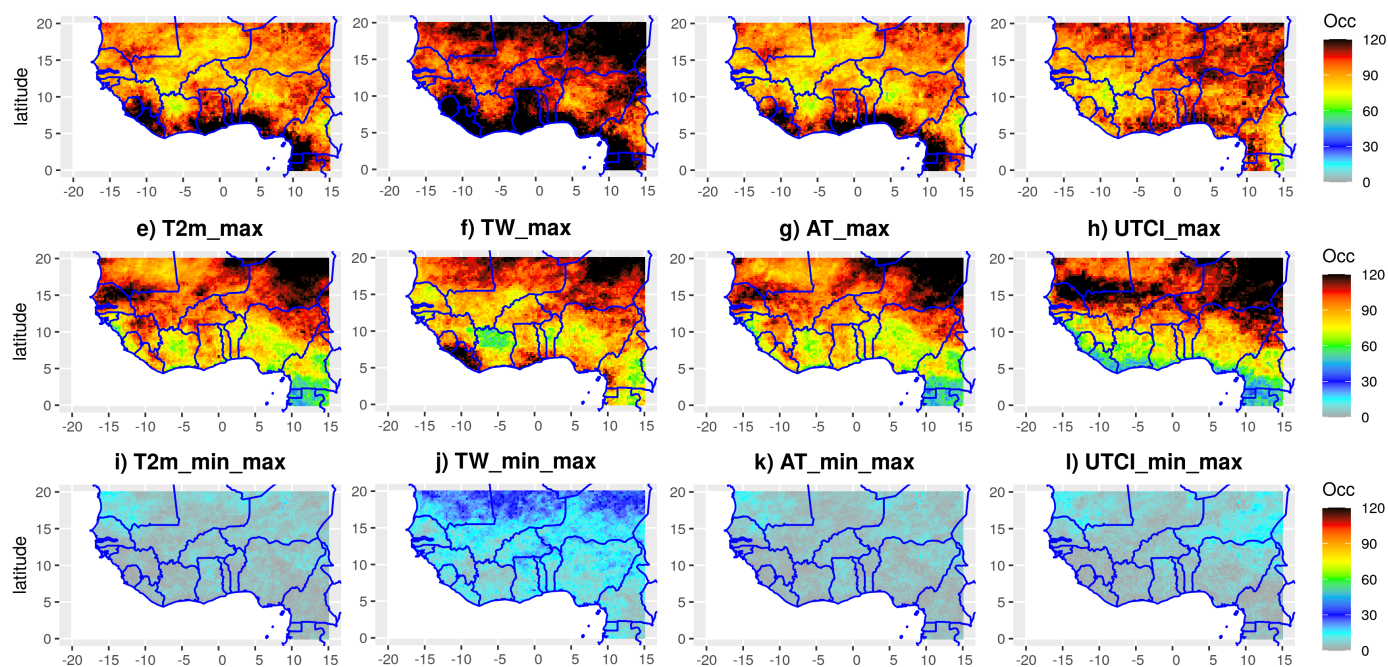
Figure 6. *Climatological state of heat wave occurrence over the period 1993-2020 using four different indicators for the heat wave detection* ($T2m$, TW, AT, $UTCI$) *with respect to the definition of heat wave : a-d) minimum values of indicators, e-h) maximum values of indicators and i-l) minimum and maximum values of indicators. The detection was processed using ERA5 and the percentile 90th as a threshold. X and Y-axis respectively represent the longitude and latitude in degrees. The color bar shows the frequency of events per region.*
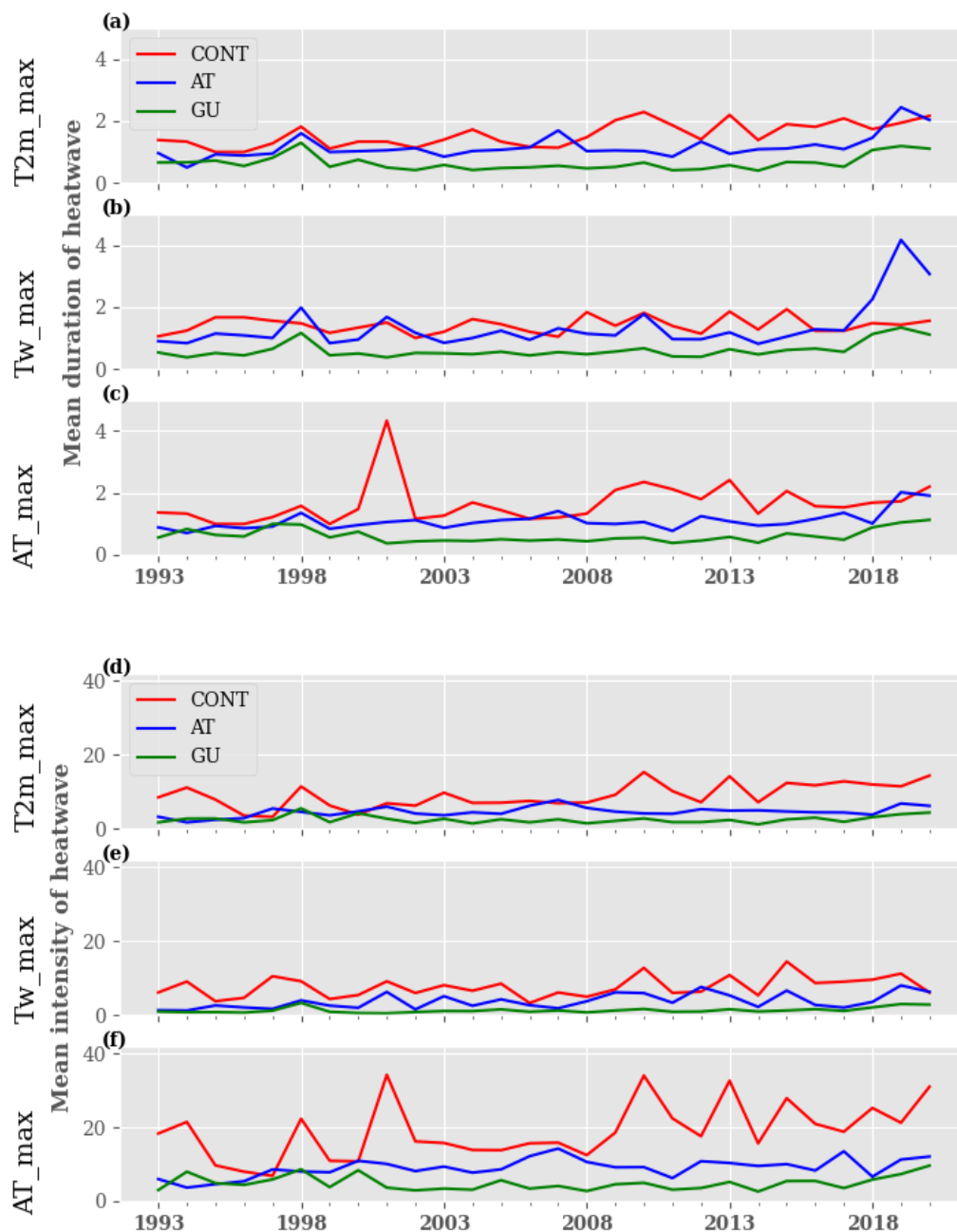
Figure 7. *Interannual variability of heat wave characteristics using maximum values of T2m, TW and AT : a-c) mean duration and d-f) mean intensity. The Y-axis represents respectively the duration and intensity of heat waves, the X-axis represents the time in year. Red/blue/green lines represent the evolution of heat wave characteristics over CONT/AT/GU regions (see region of interest section for more details).*
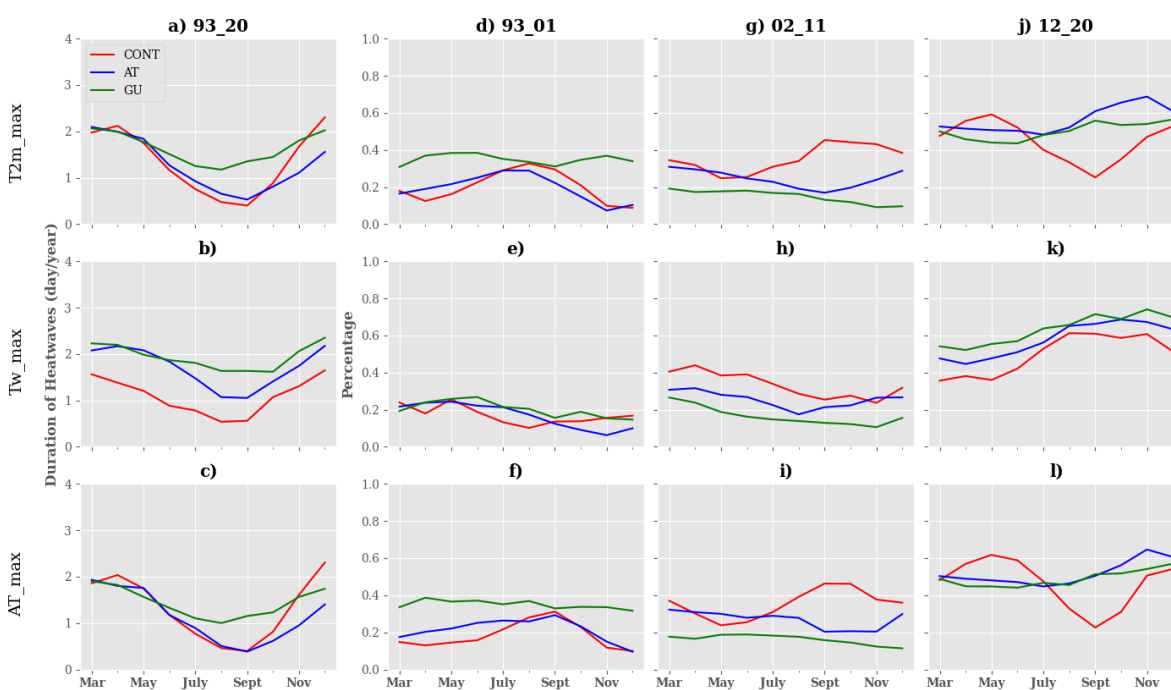
Figure 8. *Seasonal variability of heat wave yearly duration using maximum values of indicators: a) T2m, b) TW and c) AT. The first column shows the evolution of heat wave duration per year over the whole period 1993-2020. The $2^{nd}(d, e, f), 3^{rd}(g, h, i)$ and $4^{th}(j, k, l)$ columns represent respectively the contribution in percentage of the sub-periods 1993-2001, 2002-2011 and 2012-2020 to heat wave duration over the whole period. We compute a a 3-month running mean to smooth the seasonal cycle. The X-axis represents the time in days; and the Y-axis respectively the duration of heat waves, and the contribution of each decade. Red/blue/green lines represent the evolution of heat wave duration over CONT/AT/GU regions (see region of interest section for more details).*
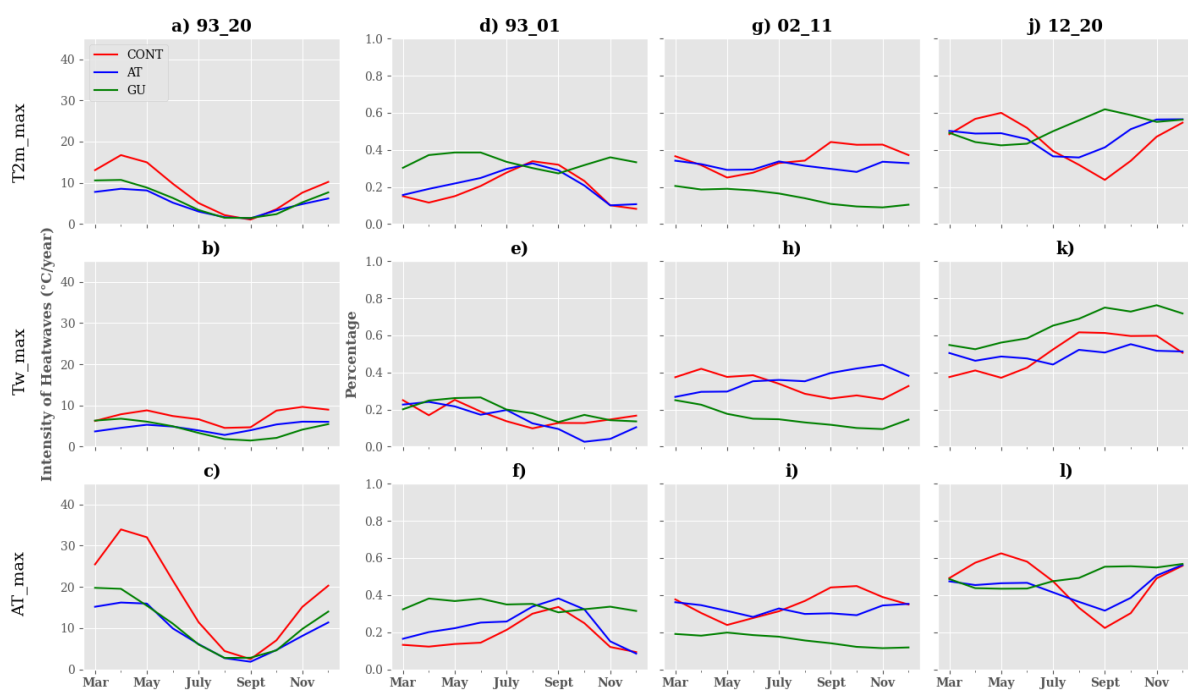
Figure 9. *Seasonal variability of heat wave yearly intensity using maximum values of indicators: a) T2m, b) TW and c) AT. The first column shows the evolution of heat wave intensity per year over the whole period 1993-2020. The $2^{nd}(d,e,f), 3^{rd}(g,h,i)$ and $4^{th}(j,k,l)$ columns represent respectively the contribution in percentage of the sub-periods 1993-2001, 2002-2011 and 2012-2020 to heat wave intensity over the whole period. We compute a a 3-month running mean to smooth the seasonal cycle. The X-axis represents the time in days; and the Y-axis respectively the intensity of heat waves, and the contribution of each decade. Red/blue/green lines represent the evolution of heat wave intensity over CONT/AT/GU regions (see region of interest section for more details).*
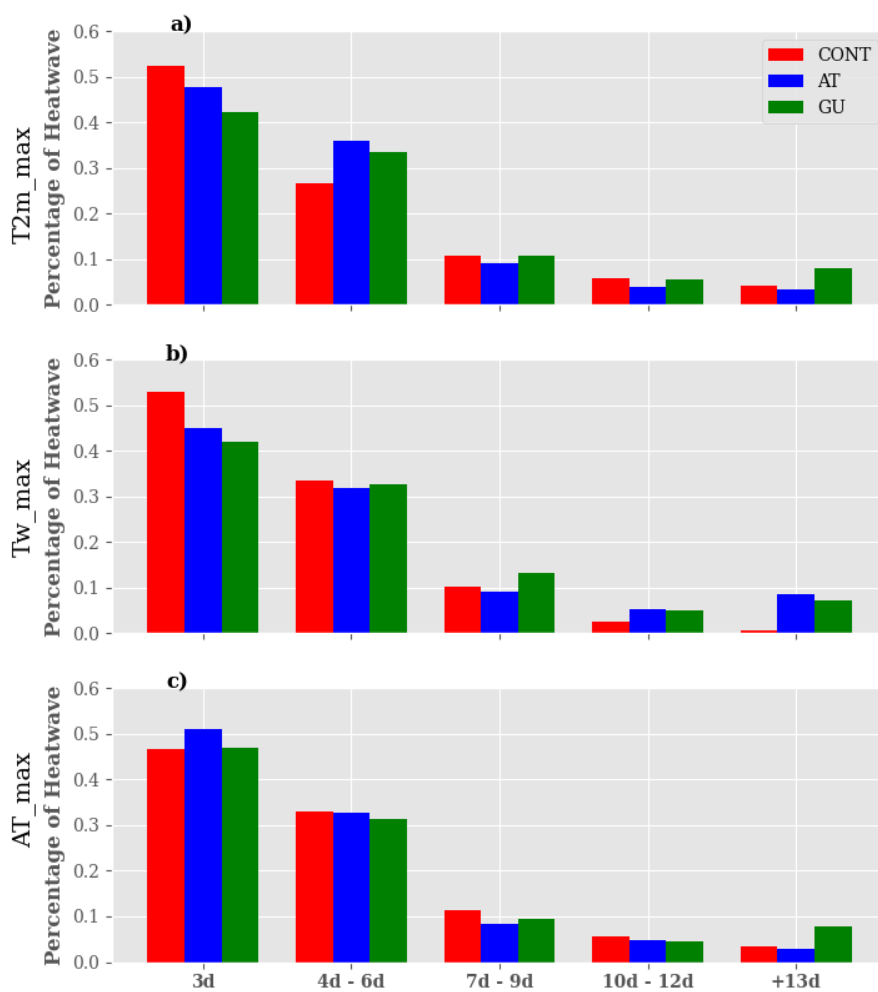
Figure 10. *Classification of the heat waves detected using maximum values of indicators based on the duration: a) $T2m$, b) TW and c) AT. The X and Y-axis represent respectively the percentage of the heat wave per class and the duration in day. Red/blue/green bars represent the percentage of heat waves detected over CONT/AT/GU regions (see region of interest section for more details).*
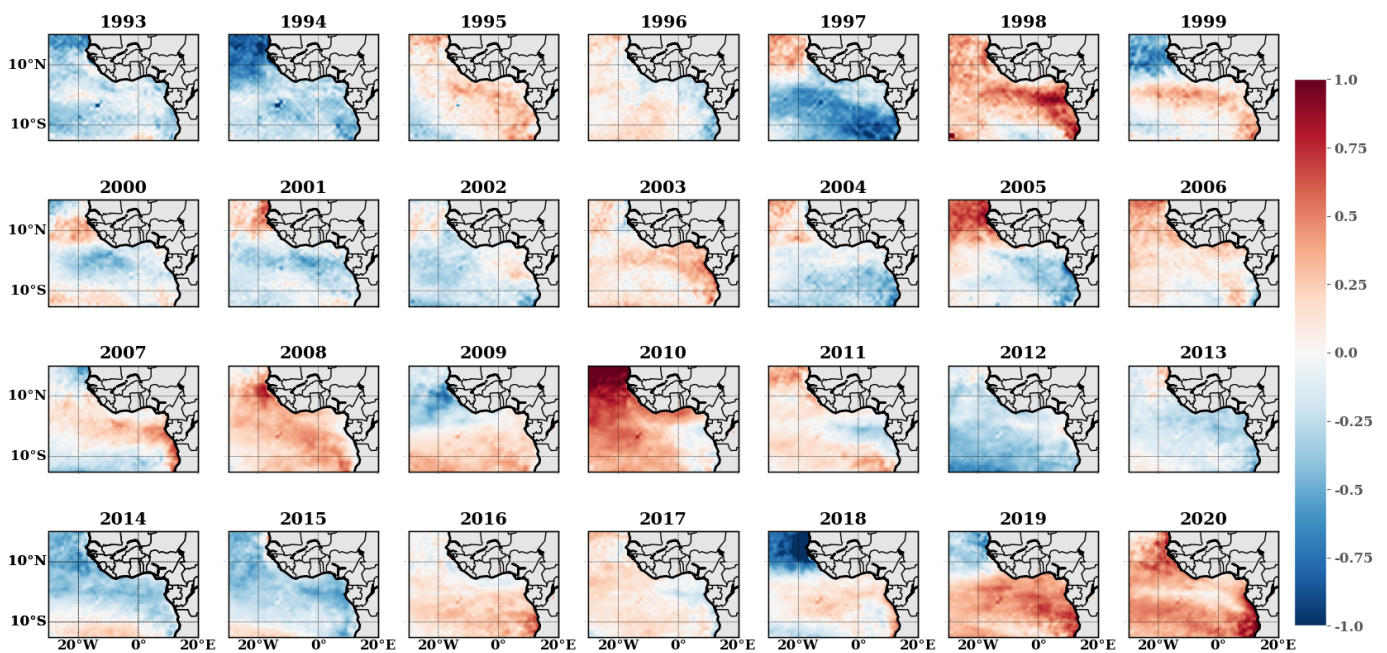
Figure 11. *Interannual variability of the sst anomalies over the period 1993-2020. The anomalies are computed as the difference between yearly sst and the climatology of the sst over the whole period. The X and Y-axis represent respectively the longitude and latitude in degree. The color bar shows the values of the anomalies in degree Kelvin.*
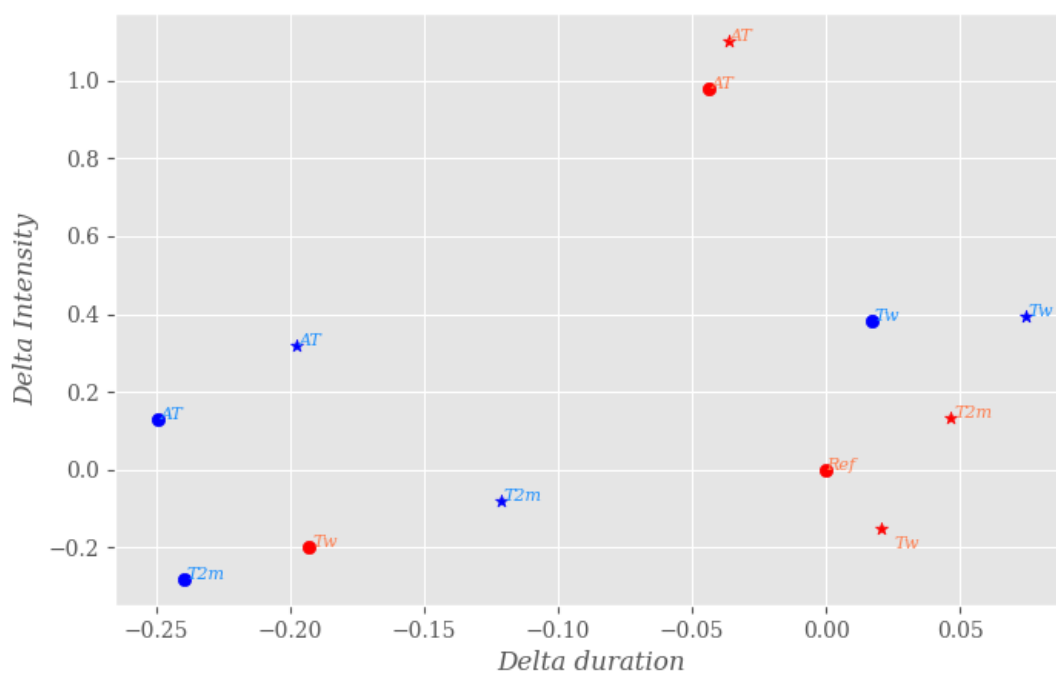
Figure 12. *Sensitivity of heat wave characteristics to the datasets, indicators and methodology used in the CONT region. The circles and stars in the figure represent respectively ERA5 and MERRA reanalyses. The blue/red color represents min/max values of the indicators. "Ref" is the reference variable used for the analysis, here "$T2m_{max}$" from ERA5. The Y- and X-axis show the standardized variation of intensity and duration respectively from the reference (no unit). The variation of duration and intensity have been computed using max daily T2m in ERA5 as reference.*